ACRS 2022
MONGOLIA

QUANTIFICATION OF TOTAL SUSPENDED SEDIMENT IN MUDA DAM USING MULTI-TEMPORAL LANDSAT OPERATIONAL LAND IMAGER (OLI)

Maizatuldura Mohd Isa[1], Shahruddin Ahmad[1], Hana Mohamed Jamil[1], Nurul Suliana Ahmad Hazmi[1] and Sabrina Shahri[1]

[1] *Malaysian Space Agency (MYSA)*
Ministry of Science, Technology, and Innovation (MOSTI)
No. 13, Jalan Tun Ismail, 50480 Kuala Lumpur, Malaysia,
maizatuldura@mysa.gov.my; shahruddin@mysa.gov.my;
hana@mysa.gov.my;nurulsuliana@mysa.gov.my; sabrina@mysa.gov.my;

KEYWORDS: Remote Sensing, Total suspended sediment, Landsat, Multi-temporal, Regression

ABSTRACT: Muda Dam is in northern Peninsular, Malaysia, as freshwater storage for water supply, irrigation, fisheries and tourism. The dam catchment is mostly covered by natural forest and silting the reservoir when logging activity begins in recent years. In this study, total suspended sediment (TSS), which affect water's turbidity, were used to determine the current status of the accumulated sedimentation in Muda Dam using multi-temporal optical remote sensing data. Suspended sedimentation will reduce the water storage capacity, thus decreasing the reservoir's effective storage capacity over time. The study objective is to determine the concentration of multi-temporal TSS in Muda Dam using Landsat Operational Land Imager (OLI) data from 2015 to 2021. Multi-temporal TSS empirical and regression modelling has been developed using individual bands, band ratios, and various band combinations. TSS map and concentration percentage were calculated to determine the regression rate and validated with bathymetry data for the loss in reservoir gross capacity due to sediment deposition for 7 years from 2015 to 2021. The results show the concentration rate of TSS increases because human activities. This study proved that the remote sensing technique is capable of monitoring water turbidity on the large scale in a short time and forecasting future TSS concentration rates which are of great significance for effective dam sedimentation monitoring.

1. INTRODUCTION

Climate change, geological processes, and land use cover (LU) directly affect fluvial systems and sediment transport (Cremon,2020). Watershed development activities including urbanization, agriculture, and forestry can influence fine sediment quantity, quality and its transport and storage regime by altering the natural timing and volume of water and sediment delivered to the stream channel (John, 2011). Fine sediment less than 2 mm is the main component of naturally functioning streams but can become a pollutant when development activities increase stream concentrations beyond that of the natural regime or when the sediments carry contaminants (John, 2011). Timber harvesting has the potential to negatively impact streams and riparian habitats by increasing nutrient inputs, elevating water temperatures, and delivering sediment to streams (Daniel,2020). One of the causes of many problems in reservoir maintenance is reservoir silting. Materials that enter the water will be suspended and accumulated (Froidefond,2003). Total suspended sediment (TSS) will increase water turbidity, which can affect water quality and precipitate reservoirs. Monitoring the process of water turbidity is difficult because the reservoir area is large and the process of the material entering the reservoir cannot be seen. This problem can be seen when floods occur due to a decrease in reservoir capacity (Yanti,2016). The concentration value of this parameter can be used as a reference in determining the level of pollution that occurs in the area (Hendrata,2019). Total suspended sediment (TSS) is a water quality parameter that can be used to understand sediment transport, aquatic ecosystem health, and engineering problems (Saad,2021). TSS is the measure of particles in the water column that carries many of the pollutants and sediment. By measuring TSS in a water body, managers can see how much of these particles were carried. As suspended particles increase in a waterbody, lights would be more scattered and harder to travel through the water column, and therefore the water's turbidity index will be higher (Hajigholizadeh,2021).

Muda Dam, Malaysia, is in the north of peninsular Malaysia as freshwater storage for water supply, irrigation, fisheries and tourism. Muda Dam experienced water depletion during the dry season due to increased sedimentation content inside the dam. Therefore, it is very important to periodically monitor spatiotemporal sediment concentrations over this area. Satellite images have great potential to monitor water quality assessment. Several studies have shown that reliable empirical relationships can be developed between Landsat Operational Land Imager data and ground observations for water quality parameters such as turbidity, total suspended sediment and chlorophyll (Arun,2011).

Substances in surface water can significantly change the backscattering characteristics of surface water. Remote sensing techniques depend on the ability to measure these changes in the spectral signature backscattered from water and relate these measured changes by empirical or analytical models to a water quality parameter. The optimal wavelength used to measure a water quality parameter depends on the substance, its concentration, and the sensor characteristics (Jerry,2003). Many studies show that the reflectance of water which was determined from optical remote sensed data is strongly correlated with the concentration of water quality parameters (Hajigholizadeh,2021).

The objective of this study is to determine the concentration of multi-temporal TSS in Muda Dam using Landsat Operational Land Imager (OLI) data from 2015 to 2021. The relationship between Landsat data and total suspended sediment concentration has been proven by many researchers utilizing remote sensing technology. Table 1 shows examples of a TSS algorithm that was developed by using various remote sensing sensors and bands. Most researchers have proposed a relationship between reflected solar radiance measured by satellite-based rebellious and field-measured total suspended sediments inside a wide range of inland and coastal waters. In previous studies, total suspended sediment remote sensing models were used by previous researchers [based on the findings from Jaelani,2016; Shahidul,2004; Zhang,2015]. However, the developed algorithms are highly regionally dependent. It is a drawback that the developed algorithm can only be applied over the study area and cannot be used in other regions. This is due to the differences in water constituents, such as sediment color, size shape, and even concentration, that could influence light absorption, scattering, and reflectance (Saad,2021).

Table 1: Review of previous TSS algorithms. For Landsat 8, the wavelength for B2,B3,B4 and B8 are 0.45–0.51, 0.53–0.59, 0.64–0.67, 0.50–0.68µm, respectively. For MSI (MultiSpectral Instrument), the wavelength for B5 is 704.5 nm. For OCM-2, the wavelength for B5 and B6 are 546–566 and 610–630 nm, respectively.

	References	Study Area	Band	TSS Algorithm
a)	Jing Zhao et al. (2020)	Hedi Reservoir	OLI Bands 3,4 OLI Bands 2,3,4	TSS = 172.191ln2(b3/b4)-190.809 ln(b3/b4) + 61.6 TSS = -16.517 x ln[[(b4) 1 -(b3)−1]b2] - 8.363
b)	Zhang et al. (2015)	Xin'anjiang Reservoir	OLI Bands 2,3,8	TSS = -191.02b4 + 36.863b3 + 172.66b8 + 4.57
c)	Muhammad Fauzi et al. (2016)	Wadaslintang Reservoir	OLI Bands 3,4	TSS= (255.78x(ratio b4/b3) - 166.89)
d)	Santiago Yepez et al. (2018)	Orinoco River	OLI Bands 5	TSS = 1.35512b5 -2.9385
e)	Wang et al. (2017)	Pearl River estuary	OLI Bands 4,5	Log b5=-0.3575 log2 (TSS) + 1.1135 log(TSS) + 0.7162 log(b4)

2. MATERIALS AND METHODOLOGY

2.1 STUDY REGION

Muda Dam is located at latitude 6° 06 '49'' N and longitude 100° 51' 9'' E in the district of Sik in Kedah state of Malaysia. Muda Dam was built in 1969 with the main function as an irrigation water storage reservoir under the Muda Irrigation Scheme to support agricultural development and the rice sufficiency policy. This dam started degrading water quality issues due to forest activity. Water quality has an impact on domestic water supply and irrigation for the Muda area in the northern area.

Figure 1: Study Area

2.2 IMAGE ACQUISITION

The acquired data was from Landsat 8, which was launched from Vandenberg Air Force Base, California on February 11, 2013 (U.S. Department of the Interior,2022). The satellite consists of Operational Land Imager (OLI) and Thermal Infrared Sensor (TIRS). Level 2 imageries were downloaded from the https://earthexplorer.usgs.gov/ website.

Table 2: Landsat 8 bands

Band Name	Wavelength Range (µm)	Resolution (m)
Band 1 Coastal Aerosol	0.43 - 0.45	30
Band 2 Blue	0.45 - 0.51	30
Band 3 Green	0.53 - 0.59	30
Band 4 Red	0.64 - 0.67	30
Band 5 Near-Infrared	0.85 - 0.88	30
Band 6 SWIR 1	1.57 – 1.65	30
Band 7 SWIR 2	2.11 – 2.29	30
Band 8 Panchromatic	0.50 - 0.68	15
Band 9 Cirrus	1.36 – 1.38	30
Band 10 TIRS	10.6 – 11.19	100
Band 10 TIRS	11.5 – 12.51	100

2.3 REMOTE SENSING DATA

Multiple date Landsat8 OLI imageries were used. The Landsat 8 satellite is the latest generation of terrestrial remote sensing satellites. Its sensors have been significantly improved in terms of imaging mode, band settings, signal-to-noise ratio, etc. Satellite data from 2015 to 2021 with different seasons were collected and processed, accept 2017 and 2020. There is no cloud free image (>70%) of the study area throughout the year.

Table 3: Summary of the satellite remote sensing data used in this study, which includes a ground-synchronized remote sensing image on 16 October 2021.

Type of Data	Image Date
Landsat 8 Operational Land Imager (OLI)	18 March 2015
	20 March 2016
	30 June 2018
	26 December 2019
	21 June 2021

2.4 RADIOMETRIC CORRECTION

Radiometric image correction is required to improve the quality of the image and improve the pixel values that do not correspond to the value of the spectral reflectance of the actual object. Radiometric corrections conducted in this study are a correction Top of Atmosphere (ToA) and Dark Subtraction (DOS). Correction to ToA changed the pixel values of the image into the reflectance values by normalizing the angle and intensity of solar energy, while the DOS correction intended to remove atmospheric path radiance. DOS correction assumes that there is a pixel containing 0% reflectance.

TOA (Top of Atmospheric) spectral radiance was calculated using the following equation.

$$\mathbf{TOA\ (L) = ML * Qcal + AL} \quad \mathbf{(1)}$$

where:
ML = Band-specific multiplicative rescaling factor from the metadata
Qcal = Quantized and calibrated standard product pixel values (DN)
AL = Band-specific additive rescaling factor from the metadata

Reflective band DN's can be converted to TOA reflectance using the rescaling coefficients in the MTL file:

$$\mathbf{\rho\lambda' = M\rho Qcal + A\rho} \quad \mathbf{(2)}$$

where:

ρλ′ = TOA planetary reflectance, without correction for solar angle. Note that $\rho\lambda'$ does not contain a correction for the sun angle.

Mρ = Band-specific multiplicative rescaling factor from the metadata (REFLECTANCE_MULT_BAND_x, where x is the band number)

Aρ = Band-specific additive rescaling factor from the metadata (REFLECTANCE_ADD_BAND_x, where x is the band number)

Qcal = Quantized and calibrated standard product pixel values (DN)

TOA reflectance with a correction for the sun angle is then:

$$\mathbf{P\lambda = \frac{\rho\lambda'}{\cos(\theta SZ)} = \frac{\rho\lambda'}{\sin(\theta SE)}} \quad \mathbf{(3)}$$

where:

ρλ = TOA planetary reflectance

θSE = Local sun elevation angle. The scene center sun elevation angle in degrees is provided in the metadata (SUN_ELEVATION).

θSZ = Local solar zenith angle; $\theta SZ = 90° - \theta SE$

2.5 CLASSIFICATION

2.5.1 Land Cover

Five (5) Landsat imageries from 2015 - 2021 were classified into four (4) main land cover classes, which are Waterbody, Cleared Land, Forest, and Road using the Support Vector Machine Classifier (SVM) classifier. All images were cloud-free except for the image in the year 2016. The image dated 20th March 2016 is the best image available for the year 2016.

2.5.2 Water

The classification was carried out to obtain the water turbidity class by Landsat 8 OLI imagery from 2015 to 2021. The classification was done with the density method based on the spectral reflectance histogram because the peak of the histogram represents the turbidity of the water. Density segmentation is one of the classification methods that can be done by selecting the overall brightness level of the existing pixel values in the image.

2.6 RESEARCH FLOW CHART

The research flowchart is shown in Figure 3.

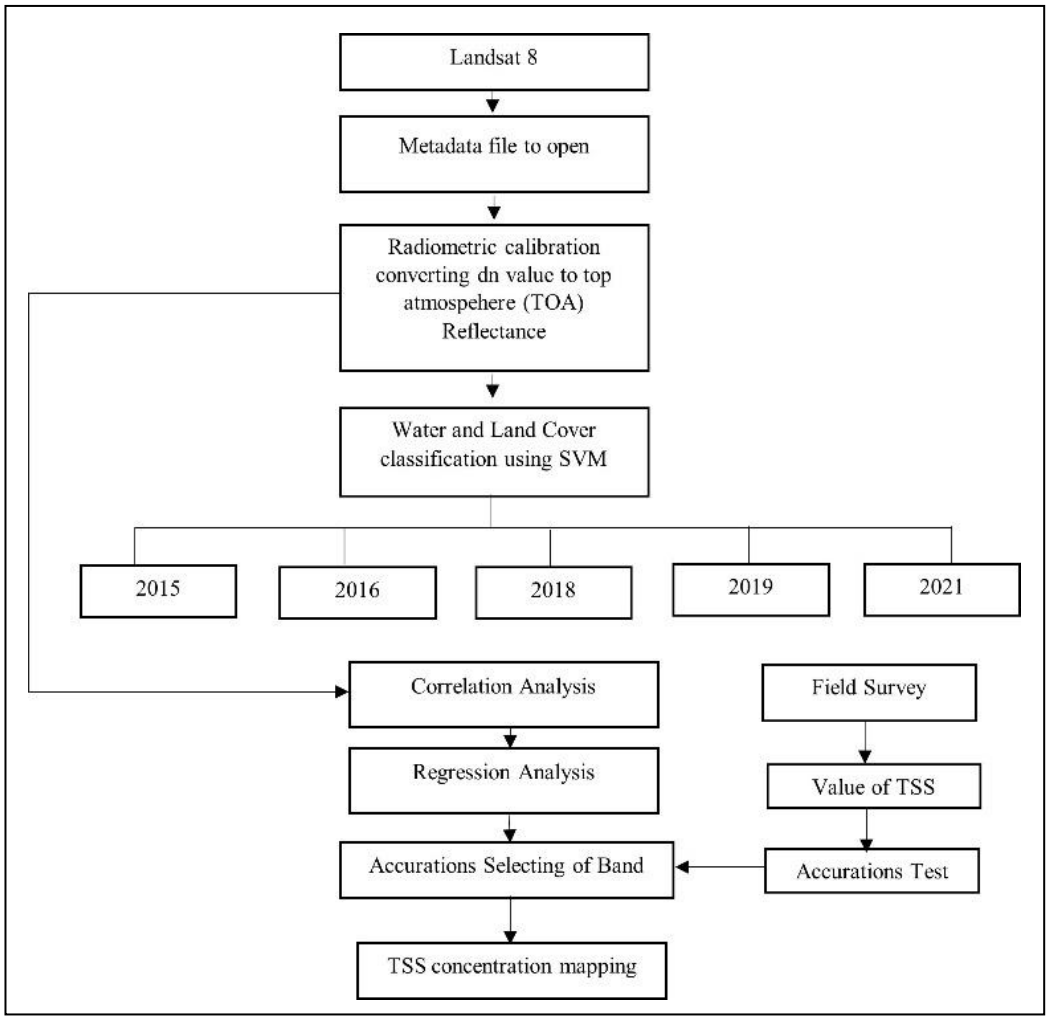

Figure 3: Research flowchart

2.7 THE PEARSON CORRELATION ANALYSIS

Correlation analysis is the relationship and direction between two or more variables. This aims to find spectral bands that have a significant relationship with the TSS field, which is required to perform regression analysis. Only spectral bands with a significant correlation coefficient (r) can be used as input in the regression analysis. The input pixel values for the empirical model are single band values, band ratio and band multiplication.

3. RESULTS AND DISCUSSION

3.1.1 MULTI-TEMPORAL LAND COVER CLASSIFICATION

The classification accuracies for year 2015, 2016, 2018, 2019 and 2021 are 96.9%, 97.4%, 92.4%, 96.3% and 97.7% respectively. Meanwhile the kappa statistics values for each year are 0.87, 0.89, 0.70, 0.83, and 0.84. The classification for this area mostly indicates good classification performance, with Kappa values more than 0.80 (based on the findings from Lillesand et al., 2004; Jensen 2005) except for the image in the year 2018 with 0.70.

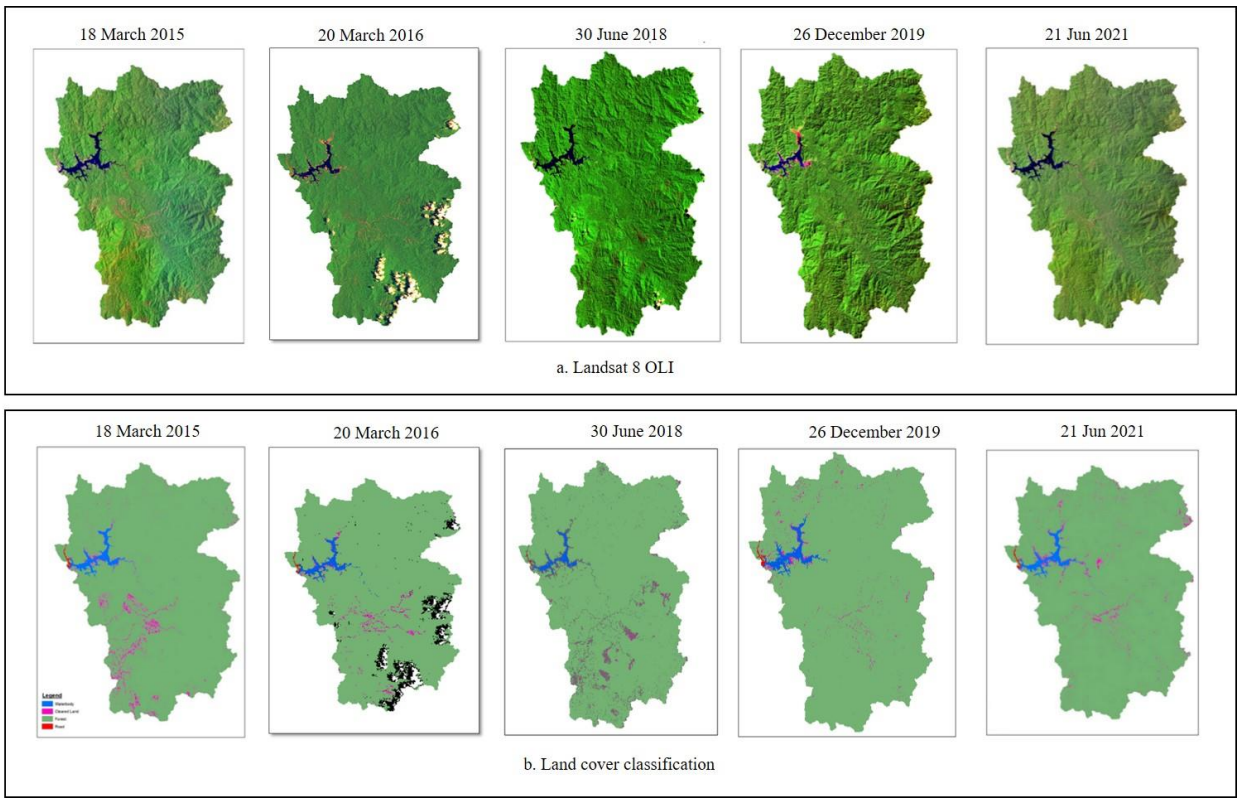

Figure 4: Land cover classification maps

Table 4: Landcover classes 2015 - 2021.

Land Cover / Year	Area (ha)				
	2015	2016	2018	2019	2021
Waterbody	1514.941	1431.224	1441.745	1612.339	1589.235
Cleared Land	2812.576	1575.799	4907.531	1327.868	2477.219
Forest	92406.965	87590.849	90385.110	93793.783	92672.448
Road	96.477	96.526	96.574	96.969	91.439
Cloud	-	3328.069			-
Shadow	-	2808.492			-

Table 5: 2015 Confusion Matrix.

Year : 2015, Overall Accuracy : 96.9 %, Kappa Statistics : 0.865					
LC	**Water**	**Cleared land**	**Forest**	**Total**	**User Accuracy**
Water	10.000	0.000	0.000	10.000	1.000
Cleared land	0.000	8.000	2.000	10.000	0.800
Forest	0.000	3.000	140.000	143.000	0.979
Total	10.000	11.000	142.000	163.000	0.000
Producer Accuracy	1.000	0.727	0.986	0.000	0.969

Table 6: 2016 Confusion Matrix.

Year : 2016, Overall Accuracy : 97.4 %, Kappa Statistics : 0.889							
LC	**Water**	**Cleared land**	**Forest**	**Cloud**	**Shadow**	**Total**	**User Accuracy**
Water	10.000	0.000	0.000	0.000	0.000	10.000	1.000
Cleared land	0.000	8.000	1.000	1.000	0.000	10.000	0.800
Forest	0.000	2.000	270.000	0.000	0.000	272.000	0.993
Cloud	0.000	0.000	2.000	8.000	0.000	10.000	0.800
Shadow	1.000	0.000	1.000	0.000	8.000	10.000	0.800
Total	11.000	11.000	274.000	9.000	8.000	312.000	0.000
Producer Accuracy	0.909	0.727	0.985	0.889	1.000	0.000	0.974

Table 7: 2018 Confusion Matrix.

Year : 2018, Overall Accuracy : 92.4 % Kappa Statistics : 0.696					
LC	**Water**	**Cleared land**	**Forest**	**Total**	**User Accuracy**
Water	9.000	1.000	0.000	10.000	0.900
Cleared land	1.000	6.000	3.000	10.000	0.600
Forest	0.000	7.000	131.000	138.000	0.949
Total	10.000	14.000	134.000	158.000	0.000
Producer Accuracy	0.900	0.978	0.977	0.000	0.924

Table 8: 2019 Confusion Matrix.

Year : 2019, Overall Accuracy : 96.4 %, Kappa Statistics : 0.831					
LC	**Water**	**Cleared land**	**Forest**	**Total**	**User Accuracy**
Water	10.000	0.000	0.000	10.000	1.000
Cleared land	1.000	6.000	3.000	10.000	0.600
Forest	0.000	2.000	143.000	145.000	0.986
Total	11.000	8.000	146.000	165.000	0.000
Producer Accuracy	0.909	0.750	0.979	0.000	0.964

Table 9: 2021 Confusion Matrix.

Year : 2021, Overall Accuracy : 97.7%, Kappa Statistics : 0.835					
LC	**Water**	**Cleared land**	**Forest**	**Total**	**User Accuracy**
Water	10.000	0.000	0.000	10.000	1.000
Cleared land	0.000	9.000	1.000	10.000	0.900
Forest	0.000	6.000	280.000	286.000	0.979
Total	10.000	15.000	281.000	306.000	0.000
Producer Accuracy	1.000	0.600	0.996	0.000	0.977

Table 10: Cleared land changes from 2015 to 2021.

Cleared Land	**2015**	**2016**	**2018**	**2019**	**2021**
Area Hectare	2812	1520	4919	1294	2477
Percentage	2.9	1.6	5.1	1.3	2.6

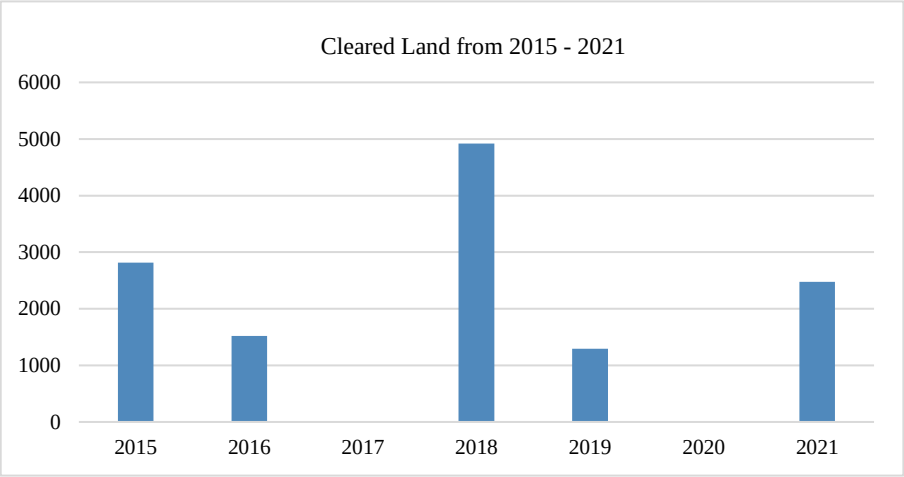

Figure 5: Graph of cleared land changes from 2015 to 2021.

The land use of the Muda Dam catchment area only consists of forest areas, therefore land use change only from forest to clear the land where logging activity by cutting on the selected tree. Image classification shows clear land increased significantly in 2018 (4919 ha) follow by 2015 (2812 ha), 2021 (2477 ha), 2016 (1520 ha) and lower in 2019 (1294 ha).

3.2 WATER QUALITY CLASSIFICATION

The spatial distribution of TSS from each band is generally similar, but the values are approximate TSS is different. This is due to the difference in the spectral reflectance properties of each band above water. Water reflection value can describe the condition and quality of water. TSS turbidity level is one of the factors of the spectral properties of water. Turbid water will have a higher reflectivity value than clear water. In principle, clear water has the highest reflectance in the green wavelength, which decreases with increasing wavelength, reaching a reflectance close to zero in the near-infrared region (Radoslaw,2015). Figure 6 shows the plot of TSS over band 5 against band 4/Band 3). The R^2 for this plot is given by 0.76. Band-ratio methods use two bands from a multispectral image and take advantage of the differences in the spectral response.

$$\mathbf{TSS = X_1[\ a\ (X_2/X_3) - b]} \qquad \mathbf{(5)}$$

where;

X_1=Band 5, X_2=Band 4, X_3=band 3

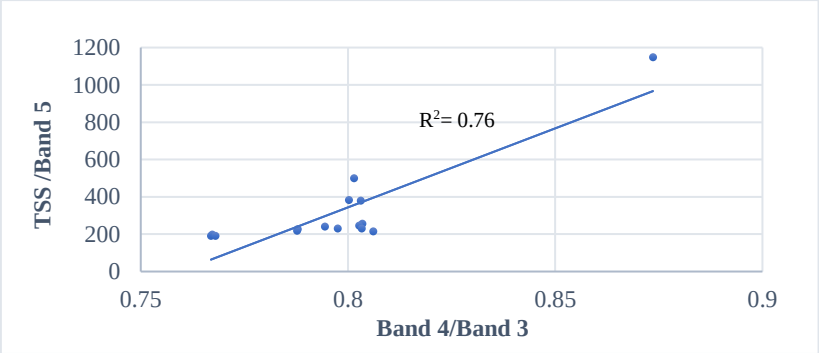

Figure 6: Regression model for TSS Concentration

3.3 MULTI TEMPRAL TSS CONCENTRATION

TSS concentration classification was done using Landsat 8 OLI multitemporal dated 18 March 2015, 20 March 2016, 30 June 2018, 26 December 2019 and 21 Jun 2021. The results show that TSS concentration changes according to changes in clear land. TSS concentration in dam reservoir highest at the inlet which transports from Muda River.

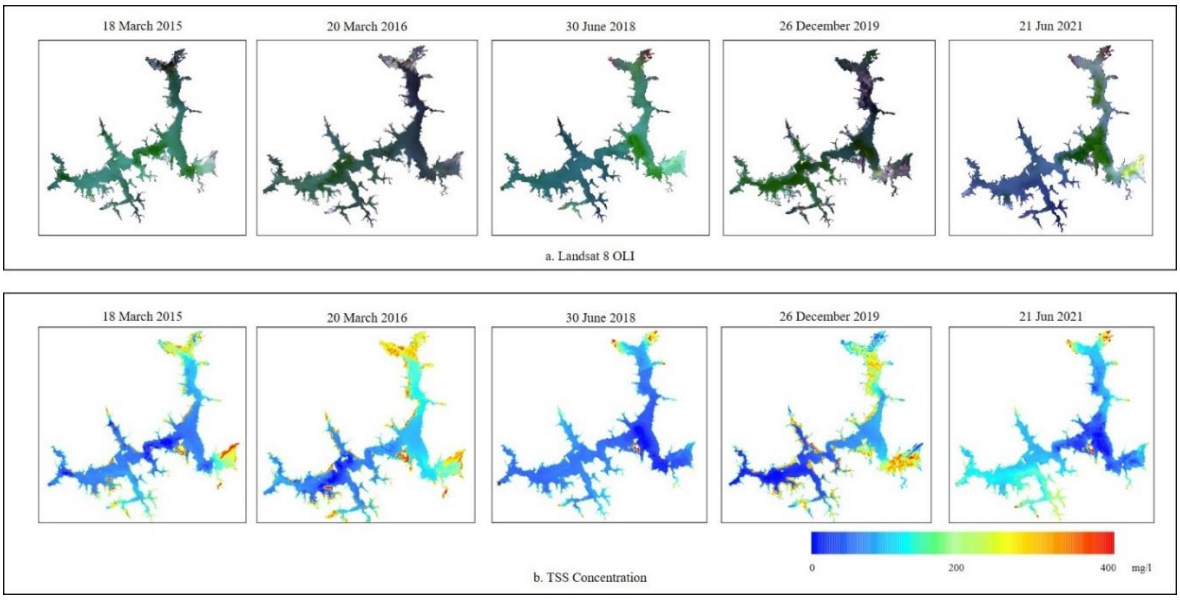

Figure 7. The Spatial Pattern of TSS Distribution Map in Muda Dam

3.4 TSS CORRELATION WITH CLEAR LAND

2019 TSS concentration was higher due to the large clear land area in 2018 (5.1 percent) compared with 2015, 2016, 2019 and 2020. The clear land decrease from 2018 to 2021 has caused the TSS concentration rate to decrease. The results also revealed that TSS concentration in 2021 has moved toward the dam wall.

2015	2016	2018	2019	2021
2812 ha	1520 ha	4919 ha	1294 ha	2477 ha
2.9 %	1.6 %	5.1 %	1.3 %	2.6 %

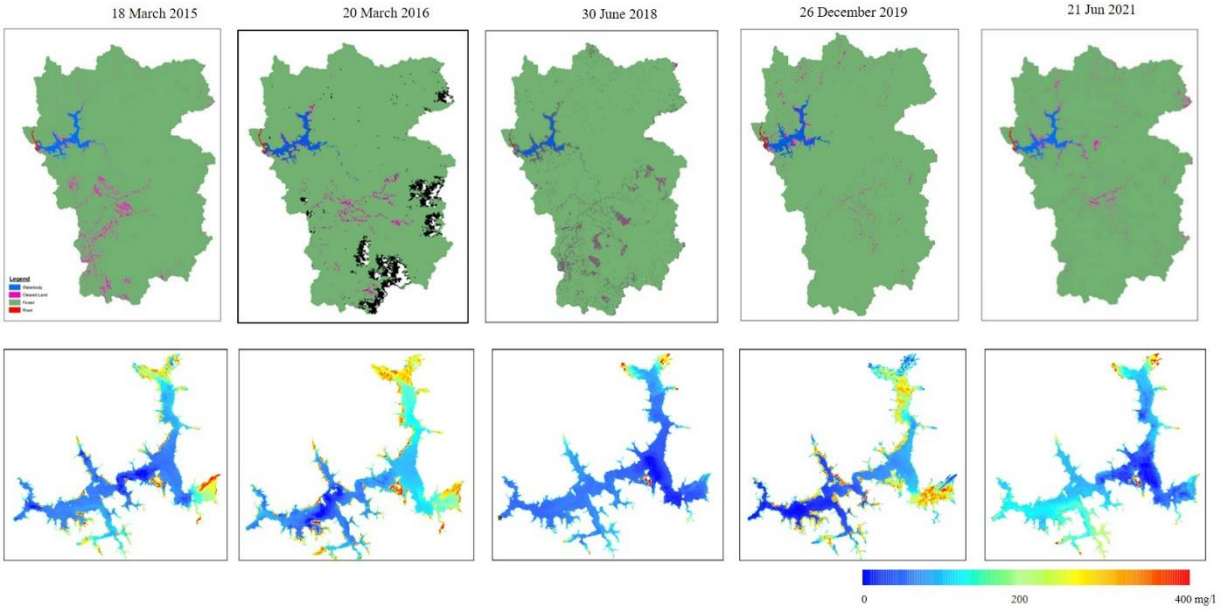

Figure 8. Multi temporal Land Use and TSS concentration from 2015 to 2021.

4. CONCLUSION

The results of TSS mapping in the Muda dam reservoir using remote sensing images show that the area with the highest TSS content is in the upstream area of the dam, at the reservoir inlet from the Muda River. The TSS spatial distribution map shows that the TSS content in the area gradually increases and accumulates in the area. Accuracy evaluation of TSS results with field tests showed that the average value of TSS in Muda Dam was 300mg/l. As a recommendation for future works, we suggest using a different location for comparison and possibly focusing on specific types of water quality for a more detailed analysis. In addition, modification of the TSS index may be required to improve accuracy.

ACKNOWLEDGMENT

The authors acknowledge EarthExplorer for the freely available Landsat 8 satellite imagery. We would also wish to thank the Malaysian Space Agency (MYSA) for the opportunity to conduct this research study.

REFERENCE

Arun, K. (2011). Water Quality Retrieval from Landsat TM Imagery. *Procedia Computer Science*, Pages 475-480.

Cremon, E. H., Montanher, O. C., & Da Sila, A. S. (2020). Estimating The Suspended Sediment Concentartion from TM/Landsat 5 Images for The Araguaia River - Brazil. *Remote Sensing Letters*, 47-56.

Daniel, B., Stringer, J., & Christopher, B. (2020). Influence of Timber Harvesting Operations and Streamside Management Zone Effectiveness on Sediment Delivery to Headwater Streams in Appalachia. *Forest*, 11, 623. https://doi.org/10.3390/f11060623.

Froidefond, J. M., Doxaran, D., & Patrice, C. (2003). Remote-Sensing Reflectance of Turbid Sediment-Dominated Waters. Reduction of Sedimet Type Variations And Changing Illumination Condition Effects by Use Of Reflectance Ratios. *Applied Optics*, 2623-2634.

Hajigholizadeh, M., Moncada, A., Kent, S., & Melesse, A. (2021). Land–Lake Linkage and Remote Sensing Application in Water Quality Monitoring in Lake Okeechobee, Florida, USA. *Land*, 147.

Hendrata, W., Bangun, M. S., & Umboro, L. (2019). Preliminary Study of Total Suspended Solid Distribution in Coastal Ujung Pangkah Gresik Based Reflectance Value of Landsat Satellite Imagery. *Indonesian Journal of Geography*, Vol 51, No1.

Jaelani, L. M., Limehuwey, R., N., K., A., P., E.S, K., & A., S. (2016). Estimation of Total Suspended Sediment and Chlorophyll-A Concentration from Landsat 8-Oli: The Effect of Atmospher and Retrieval Algorithm. IPTEK J. Technol. Sc.

Jerry, C., Paul, V., & James, H. E. (2003). Remote Sensing Technique To Access Water Quality. *Photogrammatric Engineering And Remote Sensing*, 695-704.

John, R., & Ellen, P. (2011). Fine Sediment Deposition at Forest Road Crossings: An Overview and Effective Monitoring Protocol. University of Northern British Columbia Canada. *Researchgate*, 10.5772/24275. .

Radoslaw, M., Geoff, G., Wolfgang, S., & Goswin, H. (2015). Detection and Delineation of Localized Flooding from WorldView-2 Multispectral Data. *Remote Sensing in Flood Monitoring and Managment*, 14853-14875.

Rex, J. F., & Petticrew, E. F. (2011). Fine Sediment Deposition at Forest Road Crossings: An Overview and Effective Monitoring Protocol. *Researchgate*, 10.5772/24275.

Saad, F. A., Tahir, M. S., Jemily, N. B., Ahmad, A., & Mat Amin, A. (2021). Monitoring Total Suspended Sediment Concentration in Spatiotemporal Domain over Teluk Lipat Utilizing Landsat 8 (OLI). *Remote Sensing And Geoscience Information In Applied Sciences*, 11(15), 7082.

Shahidul Islam, M., Jahangir Sarker, M., Abdul Wahab, M., Masaru, T., & Tamiji, Y. (2004). Water and sediment quality, partial mass budget and effluent N loading in coastal brackishwater shrimp farms in Bangladesh. Mar. Pollut. Bull. *Marine Pollution Bulletin*, 48, 471–485.

U.S. Department of the Interior. (2022). Retrieved from USGS Science For A changing World: https://www.usgs.gov/core-science-systems/nli/landsat/landsat-8?qt-science_support_page_related_con=0#qt-science_support_page_related_con

Wang, C.; Chen, S.; Li, D.; Wang, D.; Liu, W.; Yang, J. A Landsat-based model for retrieving total suspended solids concentration of estuaries and coasts in China. Geosci. Model Dev. 2017, 10, 4347–4365.

Yanti, A., Susilo, B., & Wicaksono, P. (2016). The Aplication of Landsat 8 OLI for Total Suspended Solid (TSS) Mapping in Gajahmungkur Reservoir Wonogiri Regency 2016. *IOP Conference Series: Earth and Environmental Science* (p. Volume 47). Yogyakarta, Indonesia: IOP Publishing Ltd.

Zhang, Y.-B., Zhang, Y., Yong, Z., & Kun, S. (2015). 14. Zhang, Y.-B.; Zhang, Y.-L.; Zha, Y.; Shi, K.; Zhou, Y.; Wang, M.-Z. Remote sensing estimation of total suspended matter concentration in Xin'anjiang Reservoir using Landsat 8 data. *Huan Jing Ke Xue Huanjing Kexue*, 56–63.